



HAL
open science

Effects of repeated drawdown flushing on riverbed fine sediment dynamics downstream from a dam

Théo Bulteau, Baptiste Marteau, Ramon J Batalla, Emmanuel Chapron,
Philippe Valette, Hervé Piégay

► **To cite this version:**

Théo Bulteau, Baptiste Marteau, Ramon J Batalla, Emmanuel Chapron, Philippe Valette, et al..
Effects of repeated drawdown flushing on riverbed fine sediment dynamics downstream from a dam.
Anthropocene, 2024, 47 (8), pp.100444. 10.1016/j.ancene.2024.100444 . hal-04803973

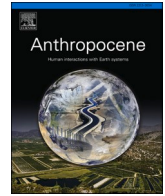
HAL Id: hal-04803973

<https://hal.science/hal-04803973v1>

Submitted on 26 Nov 2024

HAL is a multi-disciplinary open access archive for the deposit and dissemination of scientific research documents, whether they are published or not. The documents may come from teaching and research institutions in France or abroad, or from public or private research centers.

L'archive ouverte pluridisciplinaire **HAL**, est destinée au dépôt et à la diffusion de documents scientifiques de niveau recherche, publiés ou non, émanant des établissements d'enseignement et de recherche français ou étrangers, des laboratoires publics ou privés.



Effects of repeated drawdown flushing on riverbed fine sediment dynamics downstream from a dam

Théo Bulteau^{a,b,c,*}, Baptiste Marteau^{a,d}, Ramon J. Batalla^{b,e}, Emmanuel Chapron^{c,f},
Philippe Valette^c, Hervé Piégay^a

^a University of Lyon, UMR 5600 Environnement Ville Société, CNRS, Site of ENS Lyon, Lyon, France

^b University of Lleida, Fluvial Dynamics Research Group (RIUS), Lleida, Catalonia, Spain

^c University of Toulouse Jean Jaurès, UMR 5602 GEODE, CNRS, Toulouse, France

^d Rennes 2 University, UMR 6554 Littoral – Environnement – Télédétection – Géomatique, Rennes, France

^e Catalan Institute for Water Research (ICRA), Girona, Catalonia, Spain

^f LTSER France, Zone Atelier "Pyrénées-Garonne", Auzerville-Tolosane, France

ARTICLE INFO

Keywords:

RoR dam
Drawdown flushing
Riverbed clogging
TIR mapping
Upper garonne

ABSTRACT

Sediment accumulation in reservoirs is frequently a problem, impelling dam managers to implement strategies such as drawdown flushing to limit siltation. Drawdown and other sediment removal methods may induce riverbed clogging downstream of dams, especially in river sections where water is diverted, thereby reducing transport capacity. In this study, we investigate the effects of drawdown flushing downstream of the Plan d'Arem run-of-the-river dam (Upper Garonne, Spain – France border) using an adaptive inter-site comparison strategy to consider a range of spatial and temporal conditions, which allow us to separate the effects of dam storage and flushing from other potential factors. Drawdown flushing has been undertaken three times during the study period over a short span of time (2 months). We couple bed material sampling, which provides direct information on bed composition, with airborne infrared thermal imaging to better interpret whether fine sediment interstitial storage within the bed is associated with clogging. We also measure bed surface grain size and bed mobility in order to investigate their potential role in controlling fine sediment dynamics. We identify surface grain size and water diversion as the main factors controlling fine sediment spatial distribution, with coarse-grained bed-surfaces and by-passing promoting fine sediment enrichment. As a result, sites located upstream and within the by-passed reach of the Plan d'Arem dam show higher fine sediment interstitial storage than sites downstream from the by-passed reach. Results from thermal imagery demonstrate such interstitial storage does not induce clogging effect. The reaches with the most important sediment storage host a high number of cool-water patches, indicating water exchanges with the hyporheic zone. Post-flushing bed composition indicates systematic export of fine sediments from the bed matrix at all sites after the first operation, afterwards fine levels remain low after the second and the third flushing. The low impact of dam flushing in term of clogging is interpreted by the fact that the interstitial material is very sandy.

1. Introduction

In mountain streams, fine sediments (< 2 mm) are commonly transported as suspended load (Walling and Moorehead, 1989; Owens et al., 2005; Misset et al., 2019, 2021), with this transport occurring mostly during flood events (e.g. Marteau et al., 2018). These sediments partly originate from erosion within the catchment, and partly from the resuspension of sediment stored within the riverbed matrix, channel banks and floodplains (Wood and Armitage, 1997). Fine sediments form

an essential component of the sediment budget of river basins (Trimble, 1983) and as such, the infilling of and release from the riverbed matrix with fine material is a common and natural process in alluvial channels. When fine sediment infilling is excessive, either due to natural or anthropogenic factors (Owens et al., 2005), it can become problematic for species that rely on clean subsurface material to complete all or part of their life cycle (e.g. salmonids, Soulsby et al., 2001, Greig et al., 2005). The deleterious effects of excessive interstitial storage are well documented in the scientific literature (see for instance Wood and

* Corresponding author at: University of Lyon, UMR 5600 Environnement Ville Société, CNRS, Site of ENS Lyon, Lyon, France.
E-mail address: theo.bulteau@gmail.com (T. Bulteau).

<https://doi.org/10.1016/j.ancene.2024.100444>

Received 2 January 2024; Received in revised form 5 June 2024; Accepted 9 July 2024

Available online 22 July 2024

2213-3054/© 2024 Elsevier Ltd. All rights reserved, including those for text and data mining, AI training, and similar technologies.

Armitage, 1997 and Wharton et al., 2017 for reviews), and often referred to as clogging (or colmation). Clogging can be defined as the deposition of fine organic and inorganic particles on the benthic zone and their infiltration within the hyporheic zone (Gayraud et al., 2002) in gravel-to-cobble-bed rivers, leading to a reduction of pore volume, consolidation of the sediment matrix, and decreased permeability of the stream bed (Brunke and Gonser, 1997). Early attempts to describe the dynamics of this process date back to the 1980's (Bloesch and Burns, 1979; Bretschko and Klemens 1986), when anthropogenic fine-sediment inputs to river systems increased in response to the intensification of agricultural practices (Owens et al., 2005, Collins and Zhang, 2016). In brief, clogging-associated biological impacts ensue from the decreased connectivity between the surface and the hyporheic zone, which notably results in reduced intra-gravel dissolved oxygen concentrations. When this occurs, the variety and abundance of benthic macro-invertebrates and the available habitats for fish spawning and egg incubation are at risk. Moreover, clogging may persist across time because reduced intra-gravel flows are unable to flush out interstitial fine sediments, and bed-consolidation inhibits bedload transport during floods, and thus also flushing (Brunke, 1999).

However, some effects of riverbed clogging still need studying, one of these being the thermal regime of the river, which can potentially be affected by clogging (Brunke and Gonser, 1997; Packman and MacKay, 2003; Caissie, 2006), and which to the best of our knowledge, has not been specifically studied. Caissie (2006) classifies factors influencing the thermal regime into four categories: (1) atmospheric conditions (i.e. the potential amount of exchangeable energy between air and surface water) at the macroscale, (2) relief and riparian vegetation which can reduce the direct effect of solar radiance on surface temperature through shading, and in-stream flow conditions such as (3) discharge and (4) hyporheic flows which can influence surface temperature through the three-dimensional mixing of water bodies from different sources at different temperatures. The latter may be particularly affected by human activities, as water retention and diversion have profoundly affected the hydrology of rivers, with sometimes significant effects on thermal regime (Hockey et al., 1982; Bartholow, 1991; Sinokrot and Gulliver, 2000 – cited in Caissie, 2006). In addition, changes in sediment yield caused by river engineering, land use changes and even gravel mining can promote enrichment of fines over and into the bed, with potential effects on hyporheic exchanges. A loss of permeability caused by sediment infilling can reduce hydraulic conductivity within the hyporheic zone, potentially preventing the upwelling of cooler (in summer) hyporheic water towards the surface. However, groundwater inflow originating from deeper and longer pathways at the valley scale (Poole, 2010) may still be able to flush through the bed matrix and generate patches of cooler water (Schälchli, 1992) in the flow channel. The presence/absence of patches of cooler water in areas where groundwater inflows are found and hyporheic exchanges are expected can then be an indication of the presence/absence of hyporheic water exchanges, thus providing a potential method for an initial assessment of the degree of riverbed clogging.

In Europe, the Water Framework Directive adopted in 2000 aims at providing a “good ecological status” for hydrosystems by 2027, with clogging suspected to be one cause of limited achievements since 2015 (Noack, 2021). Recent developments in understanding interstitial fine-sediment storage and its release processes point towards a highly dynamic process that often shows large spatio-temporal variability (Misset et al., 2021). Consequently, assessment of the temporal dynamics of clogging often implies important field efforts with high-frequency sampling (e.g., Marteau et al., 2018) and extrapolation of field observations over long reaches, which leads to substantial uncertainties (Misset et al., 2021). The complexity of the interacting factors influencing clogging increases the difficulty of producing general clogging threshold values (above which a substrate should be considered as clogged) based on only a few measurements (Descloux, 2011). Such thresholds may be developed considering ecological aspects (e.g.,

macro-invertebrate abundance and diversity, survival of eggs; Coulombe-Pontbriand and Lapointe 2004; Seitz, 2020), or the degree of perturbation to physical functioning (e.g., thermal exchanges). Moreover, metrics that are commonly used to assess clogging (percent fines, porosity, hydraulic conductivity, O₂ level) only allow assessment of specific aspects of the process (e.g., sediment dynamics in Piqué et al., 2014 and Marteau et al., 2018; biological effects in Coulombe-Pontbriand and Lapointe 2004) within a given area that can be characterised by macro-scale (i.e., topography, hydrology, geology, nature and intensity of human disturbances), meso-scale (i.e., river morphology), and micro-scale (i.e., grain size distribution) parameters.

Furthermore, issues concerning fine sediment are increasingly important in dam management, especially in regard to accumulation within the reservoir (Annandale, 2013; Wang and Kondolf, 2014), and sometimes also downstream from the dam (Owens et al., 2005). Siltation is responsible for a loss of total reservoir storage capacity of 0.5 %–1 % yr⁻¹ worldwide (Morris et al., 2008), impelling dam managers to implement methods to limit such accumulation, such as sediment dredging and pass-through, the use of bottom-release structures, and drawdown flushing (see Kondolf et al., 2014 for details). Recent research topics involving the assessment of clogging downstream from dams include armoured sections affected by coarse sediment starvation and infrequent bed mobility, delivery of fine sediment by downstream tributaries and its accumulation in a section with reduced transport capacity (Loire et al., 2019), and drawdown flushing performed by dam managers to prevent reservoir siltation (Loire et al., 2021).

Tackling the question of clogging along river reaches requires more case-studies and methodological developments, to better link discrete field observations with larger-scale physical behaviour. Recent work in this direction has highlighted the need to use multiparameter approaches, i.e. combine methods capable of assessing different aspects of “clogging” (e.g. physical, chemical and/or biological components, Seitz, 2020). To help fill this thematic and methodological gap, we aimed to assess the effects of a dam on riverbed clogging by combining field measurements and airborne infrared thermal imagery (TIR). We focussed on the Plan d’Arem run-of-the-river (hereafter RoR) dam (Upper Garonne, Central Pyrenees, Spain–France border area) because it potentially combines two of the three processes generating clogging downstream of dams: i) sediment starvation due to sediment trapping within the reservoir, and ii) drawdown flushing operations that result in potential changes in riverbed composition. Reaches were sampled for sedimentary characteristics based on a control–impact strategy (i.e. comparing sites subject to drawdown flushing with sites that are not), while airborne TIR imagery was collected over the entire study reach at a time of low discharge and high thermal contrasts between surface and sub-surface water compartments. We hypothesised that (1) the effects of the dam on riverbed infilling could be explained by geomorphological and hydrological parameters, and that (2) TIR imagery could help interpreting whether Fine Sediment Interstitial Storage (hereafter referred to as FSIS) effectively alter riverbed permeability by reducing the number, size, and/or density of cool-water patches, which could be explained by geomorphological, sedimentary (i.e., grain size) and hydrological parameters.

2. Study area

The River Garonne (Garona) is located in the Central Pyrenees and flows over Spain and France (Fig. 1). The mountain catchment of the upper Garonne has an area of 1265 km² and encompasses a wide range of elevations from 415 to 3220 m a.s.l (Fig. 1C). The abundance of granitoids (Palaeozoic) all over the upper catchment helps explaining the large amount of sand present in the river network. The study reach starts at River Kilometre 35 (RK35), i.e. 35 km downstream from the top of the river and close to the village of Bossòst (Spain), and extends until RK66. The Pique River (the main tributary) confluences with the Garonne River at RK55, which increases both the catchment area and

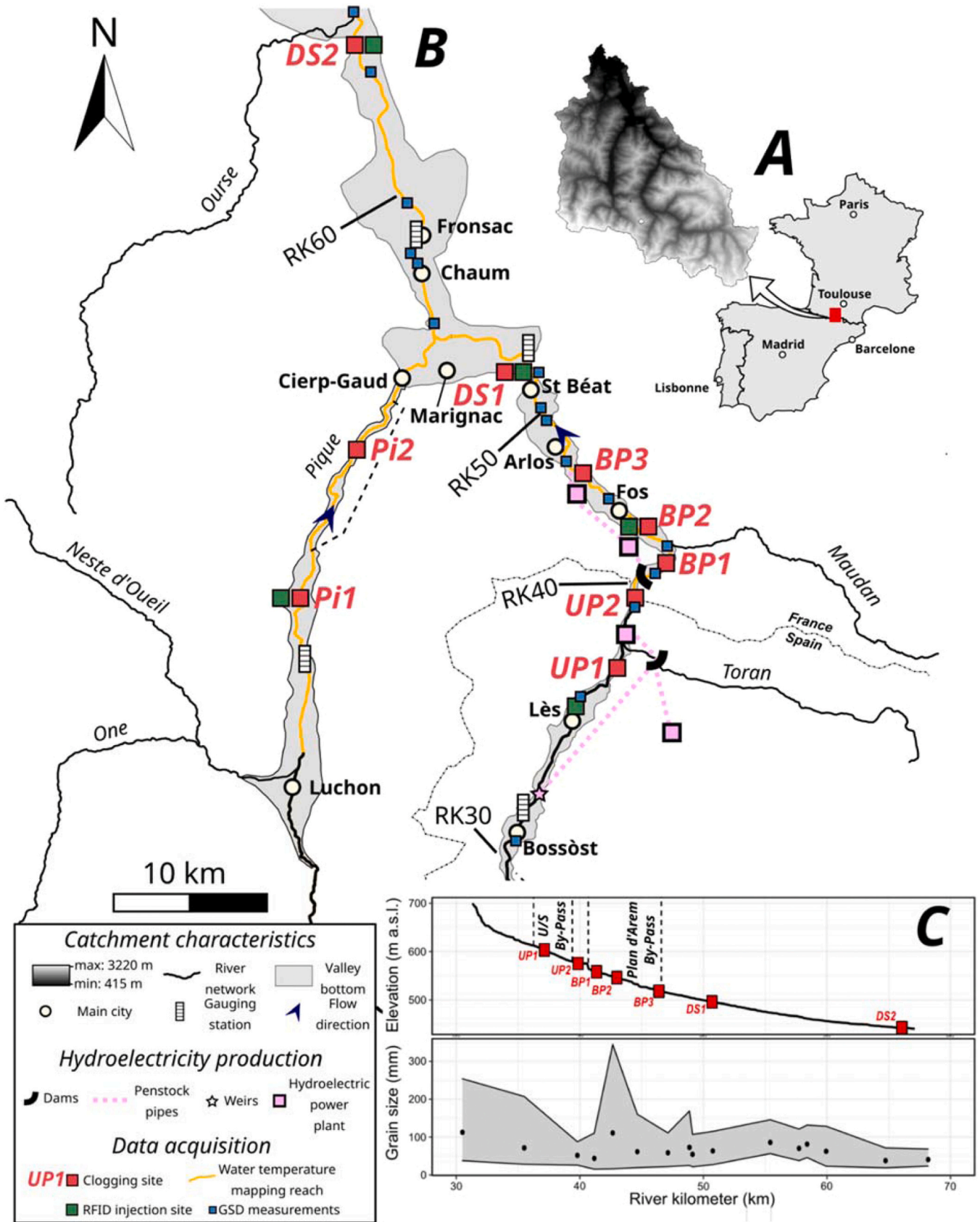


Fig. 1. A. Location of the Garonne River in Western Europe. B. Catchment characteristics and location of hydroelectric infrastructure and instrumented sites for data acquisition in the upper Garonne River. The Plan d'Arem dam is located at RK40. C. Longitudinal profile (above) and grain size distribution (below): dots represent D_{50} , grey ribbon symbolises the D_{10} - D_{90} range.

annual water yield by around 50 %. From the upstream limit of the study site to the village of St Béat (RK50), the Garonne River flows within a narrow valley less than 1 km wide, with alternation of wider reaches and a narrower glacial lock. Downstream from St Béat, the valley widens significantly, especially in the Marignac and Fronsac basins (RK53–56 and RK58–63, respectively), where the valley width reaches up to 3 km.

In the catchment headwaters, a network of dams (built between 1955 and 1965) and penstock pipes feed successive hydropower plants, (hereafter HPP), completely by-passing the natural channel until RK39 and producing hydropeaks (Fig. 1B). Further downstream, the Plan d'Arem RoR dam located at RK40 started operation in 1970, and is the only dam directly impounding the mainstem of the Garonne. The dam has two functions: to feed the two downstream HPPs of Fos and Arlos (Fig. 1B), and to buffer the effect of upstream hydropeaking by delivering a smoothed hydrograph to the Garonne. From this dam, water travels to downstream HPPs through a penstock pipe and an aerial canal, after which it returns to the river. The main channel is by-passed for 6 km, with an ecological discharge of $4 \text{ m}^3 \text{ s}^{-1}$. Because of its size and position on the Garonne mainstem, the Plan d'Arem dam disrupts sediment conveyance (Bulteau et al., 2022). Moreover, diversion of water for electricity production also affects the river's hydrology (as is the case for the upstream by-passing) by decreasing base and peak flows by up to $34 \text{ m}^3 \text{ s}^{-1}$ (i.e., 37 % of a biannual return flood), which represents the maximum operating discharge of the Fos-Arlos hydroelectric complex (i.e., maximum discharge that is by-passed when flow entering the reservoir are between 4 and $70 \text{ m}^3 \text{ s}^{-1}$; minimum flow is $4 \text{ m}^3 \text{ s}^{-1}$ and flushing flows occur $>70 \text{ m}^3 \text{ s}^{-1}$). When the construction of the dam and the derivation canal was achieved in 1970, the water storage capacity was 0.35 hm^3 . Since then, the dam reservoir has been continuously filling with sediments, mostly fine sand, silt, and clay. After over 40 years of operation, its capacity was reduced to a critical value of 0.053 hm^3 in 2013, leading managers to dredge sediment and implement drawdown flushing actions to reduce sediment accumulation. When discharge exceeds $70 \text{ m}^3 \text{ s}^{-1}$ (ca. 1-year flood), operators stop electricity production and open the bottom gate to lower the lake level and maximise sediment transfer, thereby restoring critical slope conditions. Drawdown flushing actions have minimised the effects of the dam on the downstream reach, since they have no impact on peak flows and a relatively low impact on sediment transfer, while limiting sediment accumulation within the dam lake (Bulteau et al., 2022). The recent hydrology of the Garonne River was marked by an exceptional flood on June 18th 2013, when discharge peaked at $350 \text{ m}^3 \text{ s}^{-1}$ at St Béat, which corresponds to a 100-year return period flood. This flood followed over one century of channel narrowing, bed incision and coarsening, landscape simplification and vegetation encroachment because of upstream damming and afforestation (Bulteau et al., 2022). The 2013 flood had major morphological effects, with major sediment inputs from upstream, from the slopes (reactivation of torrential production) as well as from the banks, together with a complete reshaping of the channel planform (i.e., active channel widening, bank erosion, development of alternate mobile gravel bars, etc). The effects were more the closer to Plan d'Arem dam and appear to have remained since 2013, likely thanks to drawdown flushing.

The Garonne River channel presents various degrees of geomorphic activity over the study reach, with the by-pass reach (hereafter BPR) showing higher diversity and dynamism than sections downstream of the restitution. The BPR is characterised by a relatively wide active channel due to active bank erosion processes, with gravel bars occupying 21 % of the active channel. Furthermore, this reach presents only limited bed incision. Reaches within the lower half of our study area show mainly straight channels, significant incision, and a low proportion of gravel bars (ca. 10 %; Bulteau et al., 2022).

3. Material and methods

3.1. Site selection and sampling strategy

To assess the effects on the riverbed of the Plan d'Arem dam and the associated by-passing on fine sediment dynamics with a focus on clogging, a multi-control–impact sampling strategy was undertaken. This strategy relied on selecting sites upstream from the dam (UP1–2; Control 1), within the by-passed reach (BP1–3; Impact 1), and downstream of the restitution, in other terms, where the diverted water returns to the river mainstem (DS1–2; Impact 2). To this scheme, we added two other sites on the Pique River (Pi1–2: Controls 2 and 3): one in a full-discharge reach, and the other in a by-passed reach. The nine selected sites (Fig. 1) are presented in Table 1, and were sampled on between two and eight occasions between April 2019 and November 2021, according to the river hydrology and dam operations (Fig. 2). Hydrological data from the stations of Bossost, Fos, St Béat, Chaum, and Cier-de-Luchon (Fig. 1; sources: SAIH Ebro, EDF, HydroPortail) were compiled at a 1-hour resolution. Since riverbed sediment storage often shows large variability depending on the sampled morphological unit, we chose to systematically sample glides because this unit typically shows less variability than riffle-pool sequences (Marteau et al., 2018). To characterise potential intra-site variability, three samples along a transect were taken for each site and for each sampling occasion. We further assessed local variability at sites UP1 and DS1 by taking seven and eight samples, respectively, in a 4 m^2 grid during the campaign of November 2021.

3.2. Sedimentary analysis

3.2.1. Fine sediment interstitial storage (FSIS)

In this study, fine sediments correspond to sediments smaller than 2 mm. This class is subdivided into two sub-classes. Sediments with a size comprised between 0.05 mm and 2 mm are referred as “sands”. Sediments smaller than 0.05 mm are referred as “silts and clays”. We justify the choice of the silt-clay upper limit by its closeness with the upper limit defined in the Wentworth scale (0.063 mm; Wentworth, 1922) and the very low proportion of this fraction in the streambed (see Section 4.1.1.). In the case of the Garonne River, sand is expected to be the dominant riverbed infilling material. We propose to investigate the spatio-temporal pattern of each sub-class as they may not have the same effect on hyporheic flows, in relation with the cohesive nature of silts and clays on one side, and the granular nature of sands on the other.

The fine sediment proportion of the riverbed was estimated using a method that moreover allowed sampling of the entire grain size distribution (hereafter GSD) over a defined area. This involved a hybrid method (Fig. 3A) that combined manual sampling for coarse sediments (McNeil and Ahnell, 1964; Rex and Petticrew, 2011) with water sampling for finest fraction (silt-clay, considered as suspended sediments) (Lambert and Walling, 1988; López-Tarazón et al., 2011; Piqué et al., 2014; Marteau et al., 2018). This method relied on a cylinder-corer of 16 cm diameter and 70 cm in height with 2 cm-long teeth at the bottom, adapted from the method developed by McNeil and Ahnell (1964). Prior to bed material sampling, a 500-mL clear water sample was taken and considered as a blank to assess the suspended sediment concentration of the river. This concentration was subsequently subtracted to the concentration of the test water samples. Three samples were collected at each site and on each occasion, distributed laterally (left, centre and right side of the channel). The sampler was driven into the streambed to a depth of approximately 15 cm to isolate the sampled area from river flow, thus limiting the fine sediment losses during sampling. Therefore, fine sediments (silt and clay) losses were only observed while driving the sampler in the streambed, but these losses were not observed subsequently. Bed sediments contained in the sampler were manually removed into a clean bucket until the upper limit of the sampler teeth was reached. The water column in the sampler (Dw, Fig. 3A) was

Table 1
Characteristics of the sediment sampling sites.

Site	Position	Flow regulation	Location relative to Plan d'Arem	Channel slope	D ₁₆ (mm)	D ₅₀ (mm)	D ₈₄ (mm)	Moment of sampling	Number of samples
UP1	42°49'47.6"N 0°43'42.9"E	By-passed	Upstream	0.008	21	64	179	S5–8	8
UP2	42°51'04.4"N 0°44'07.3"E	Full discharge	Upstream	0.005	25	51	87	S1–6 & S8	18
BP1	42°51'32.1"N 0°44'46.1"E	By-passed	BPR	0.007	11	39	106	S5–8	9
BP2	42°52'06.5"N 0°44'29.4"E	By-passed	BPR	0.007	11	74	240	S1–7	18
BP3	42°53'13.4"N 0°42'47.0"E	By-passed	By-pass reach	0.007	-	-	-	S1–3 & S5	11
DS1	42°54'56.6"N 0°41'29.3"E	Full discharge	Downstream	0.007	27	63	115	S1–8	21
DS2	43°00'41.3"N 0°36'59.1"E	Full discharge	Downstream	0.002	20	39	69	S1–8	20
Pi1	42°50'44.6"N 0°36'07.9"E	Full discharge	Other river	0.004	26	44	77	S1–7	21
Pi2	42°53'53.2"N 0°37'33.8"E	By-passed	Other river	0.01	29	77	134	S5–6	6

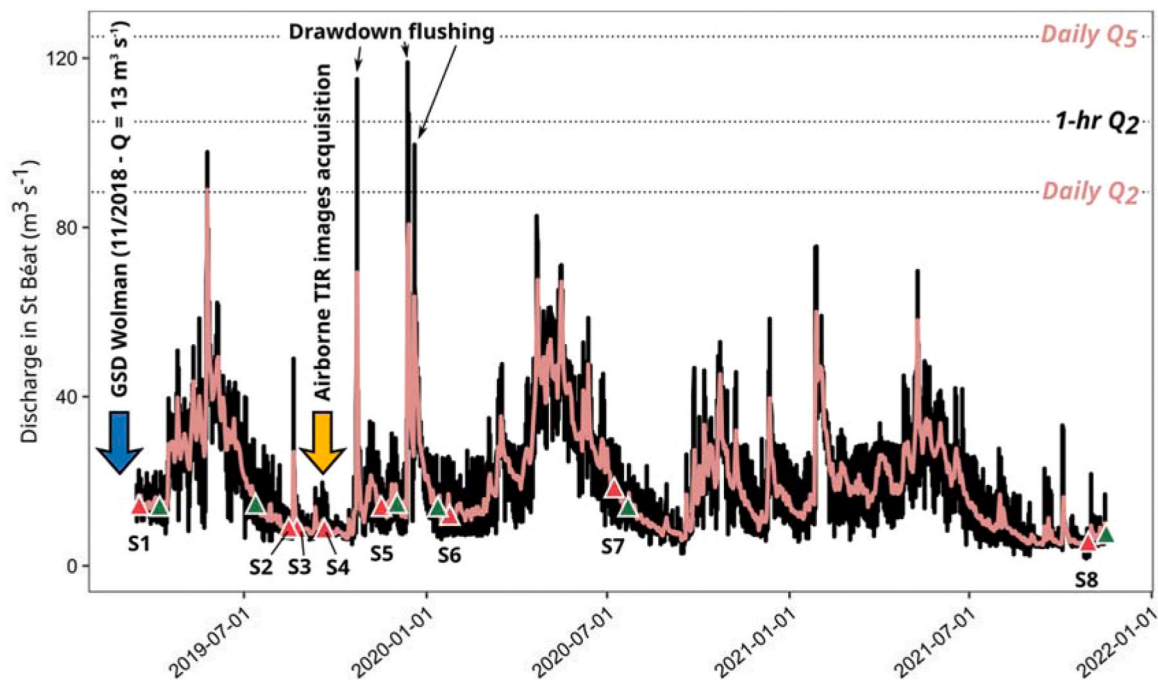


Fig. 2. Hydrology over the study period and field campaigns for clogging measurements (Survey 1 to Survey 8; red triangle), RFID surveys (green triangle), GSD, and TIR mapping (the various techniques are described in the following sections). Black line: 1-hour discharge. Red line: daily mean discharge. Dashed lines: selected reference flood return-periods.

measured and two replicate samples of 500 mL of turbid water were taken after stirring and waiting for around 10 seconds (i.e., for the sand to re-deposit; [Misset et al., 2021](#)). Immediately after sampling, the collected coarse sediments were wet-sieved at 64, 45, 32, 22, 16, and 8 mm. Before weighing, each fraction was cleaned with clear water to collect any sand and finer particles that may have remained stuck to coarser material. Material finer than 8 mm, typically representing 0–2 kg of the sediment per sample, was then brought to the laboratory for drying at 130°C for 4 hours, followed by dry-sieving at 4, 2, 1, 0.5, 0.25, 0.125, and 0.05 mm. Water samples were filtered using 1.2- μ m glass microfiber filters. The filters were dried at 110°C for 4 hours and weighed to determine the concentration in the samples. The quantity of fines released from the bed was then calculated as follows ([López-Tarazón et al., 2011](#)):

$$B = C \times V \quad (1)$$

where B is the quantity of fines released from the bed (in kg), C is the concentration in the samples (in kg L^{-1}), and V is the volume of water in the corer above the sediment surface (in L).

The sediment mass calculated from the water sample filtration was added to the grain size distribution obtained from the finest fraction (< 0.05 mm) of the coarse sediment sieving. Calculation of the percent of fines (< 2 mm) required prior truncation of the sample at 64 mm ([Rice, 1995](#); [Bunte and Abt, 2001](#)).

Considering the high variability in FSIS between sites, assessment of the temporal trends required a nondimensionalisation of the observations. To do this, a simple min-max procedure was used, given its simplicity and its relevance to our data (Eq. 2). P_1^* gives a value between 0 and 1 that reflects the proportion of the considered fraction of a given

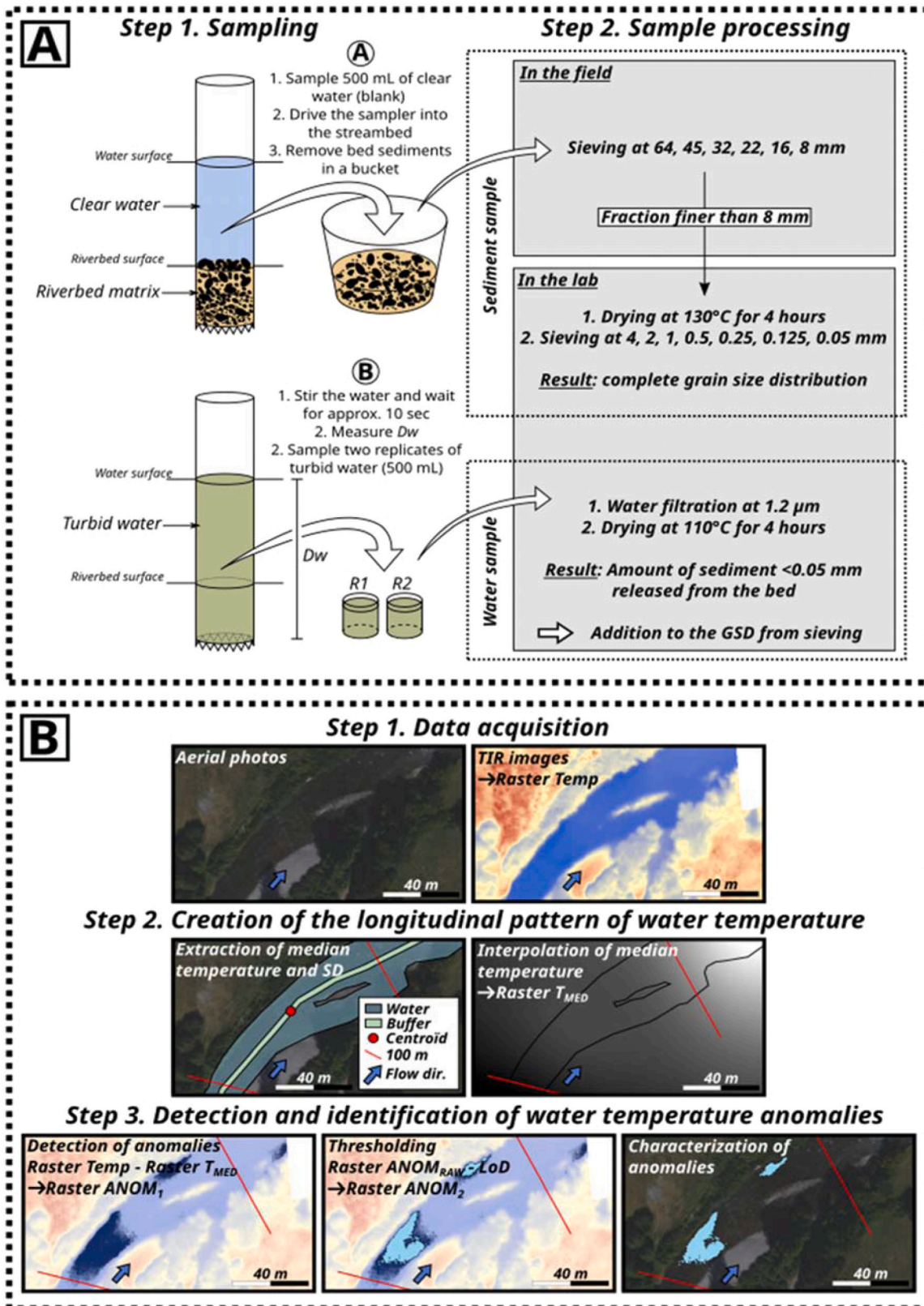


Fig. 3. A. Method for estimating bed grain-size and the fine sediment proportion. B. Method for characterising the temperature over a study reach.

site at a given date in comparison with the minimum and maximum values observed at that site over the entire study period:

$$P_i^* = \frac{P_i - P_{\text{MIN}}}{P_{\text{MAX}} - P_{\text{MIN}}} \quad (2)$$

with P_i^* = the nondimensionalised proportion of the considered fraction for a given site and sample, P_i = the proportion of the considered fraction for a given site and a given sample, P_{MIN} = the minimum proportion of the considered fraction for a given site, and P_{MAX} = the maximum proportion of the considered fraction for a given site.

3.2.2. Bed texture and mobility

The surface GSD is known to influence near-bed flow conditions, having significant effects on bedload mobility and FSIS (Staudt et al., 2017; Raus et al., 2019). We assessed GSD over the study reach by sampling 20 bar heads in winter 2019, picking 100 particles (Wolman, 1954; Rice and Church, 1998; Bunte and Abt, 2001) on both surface and subsurface layers (Buffington, 1996). Bed mobility can be an important factor influencing FSIS and the release of sediment from the streambed. The sediment sampling sites were then equipped with natural passive radiofrequency identification (RFID) tracers and resurveyed on three to five occasions to determine critical discharges (Fig. 2). Field data helped in calibrating a generalised threshold model (GTM) (Recking, 2016; Vázquez-Tarrío et al., 2019) that allowed determination of critical discharge for various size classes, and the computation of the frequency of exceedance of these threshold over the study period. Together with passive RFID tracers, active RFID tracers were injected into the substrate column (seven particles, z-axis = 30 mm, column height = 210 mm) to assess the maximum active layer between April 2019 and November 2021 (Brousse et al., 2018; Boutault, 2020).

3.3. Surface temperature mapping

3.3.1. Data acquisition

Airborne Thermal Infrared (TIR) remote sensing has successfully been used to map river surface temperature over long reaches during the last two decades (see review by Dugdale, 2016). As stated in the introduction, it is known that riverbed clogging may disrupt surface-subsurface water interactions, notably the upwelling of colder groundwater and hyporheic flows. Mapping of river temperature can thus be used to identify, localise, and characterise the presence/absence of cool-water patches (also called thermal anomalies) generated by upwelling. To maximise the temperature contrast between surface and subsurface water (i.e., to better distinguish temperature anomalies), the TIR survey was carried out during a warm summer day (15/09/2019, up to 27.4°C in Bagnères-de-Luchon, close to the study area, see details in www.infoclimat.fr) at around 13:00 central European time. A thermal imaging camera (VarioCam HR Research 600®, InfraTec GmbH, Dresden, Germany, 640 × 480 pixels) with a standard 30-mm lens and a Reflex camera (D7000, Nikon®, 4928 × 3264 pixels) with a 35-mm lens were mounted on an autogyro (ELA® 07 S) to collect both thermal images and classic (RGB) photographs. Both sensors were set to take images in time-lapse mode every 1–2 s. The survey lasted for 1 hour (12:35–13:35), long enough to cover the entire study reach back and forth to ensure sufficient overlap. The thermal images were corrected for differences in the ‘true’ kinetic temperature using an empirical calibration ($R^2 = 0.87$) comparing radiant temperature (from TIR images) with temperature measured by 15 submerged VEMCO Minilog II® loggers placed in the river (~10 cm below the surface, logging at 5-minute intervals) over the entire survey. For more details on the airborne TIR survey, see methods in Marteau et al., (2022a),b).

3.3.2. TIR data processing

Both RGB and thermal orthomosaics were created separately using structure-from-motion photogrammetry (SfM) with Agisoft

MetaShape® software (version 1.6.0), and were exported at 0.1 m pixel⁻¹ for the RGB orthophotographs and 0.4 m pixel⁻¹ for the thermal orthomosaic (Fig. 3B – Step 1). After manual digitisation of the main channel components (active and wetted channels, gravel bars, islands), the channel centreline was automatically detected using the FluvialCorridor 10.1 ArcGIS® toolbox (Roux et al., 2015). To produce a longitudinal temperature profile, a 3.2-m-wide buffer was created along this centreline and segmented at 100 m steps (Fig. 3B – Step 2). The median temperature and standard deviation were extracted for each polygon.

The main goal of the TIR mapping was to detect cool-water patches, used to assess open water exchanges between subsurface and surface and so representing a proxy of a more or less clogged riverbed. To do this in a semi-automated way, the surface temperature was compared with the local median temperature determined above (at 100 m steps), and areas cooler than the local median were considered to be thermal ‘anomalies’. However, only anomalies below a threshold of 0.43°C were considered as cool patches. Calculation of this threshold was approached as a limit of detection, and was based on known uncertainties stemming from camera accuracy, empirical correction, and local variability (see Supp. Mat. in Marteau et al., 2022b for more details on the threshold calculation). Cool-water patches were then individually classified from the orthophotographs according to their shape, size, and position within the channel (Fig. 3B – Step 3). We differentiated four types of cold patches likely to provide information on the presence/absence of clogging, with inspiration from Torgersen et al. (2012) and Wawrzyniak et al. (2016). ‘Riffle exfiltration’ refers typically to water that infiltrates upstream of a riffle crest and exfiltrates downstream (i.e., upwelling), after circulating within the hyporheic zone. A ‘lateral seep’ can be observed along the banks at the channel margin, and corresponds to groundwater input into the channel. Although not directly influenced by clogging, lateral seeps are dominant where riverbed incision is high and hyporheic control is low. ‘Bar exfiltration’ is somewhat similar to riffle exfiltration but with cool water coming from inside-bar flows and exfiltrating along the bar margin. A ‘pool’ corresponds to cold water coming from a stratified pool.

3.3.3. Segmentation

Analysis of the longitudinal temperature profile was first performed by looking at changes in thermal gradients. To do this, the temperature profile was segmented into sections of homogeneous gradient or “trend” using the EnvCpt® package in R (Killick et al., 2021). The resulting segmentation was further tested for changes in variance, which could indicate changes in underlying processes, despite a constant trend or gradient. Finally, geographical constraints were added when necessary to simplify the analysis, such as those associated with the restitution of diverted water and a confluence with a major tributary. The thermal gradients and cool-water patches characteristics were then analysed for each sub-reach and linked with the geomorphological variables at the different scales to assess how these parameters could help interpret the degree of alteration caused by clogging from a “functional” perspective.

3.4. Geomorphic analysis

A dataset from Bulteau et al. (2022) was used to characterise the local-to-large-scale geomorphic settings and assess their potential for controlling fine sediment dynamics and water temperature patterns. The river planform (namely, active channel width, wetted channel, and vegetated islands) was digitised from the orthophotographs (see Section 3.5). Gravel bars were then extracted by subtracting the wetted channel from the active channel area. Valley width was digitised from aerial photos taken in 2016 (French National Geographic Institute) when discharge was low ($Q \sim 13 \text{ m}^3 \text{ s}^{-1}$). Patterns of vertical evolution were extracted from two low-flow long profiles of water surface elevation taken in 1922 and 2014, following Liébault et al. (2013). Both were measured in September month, $Q < 30 \text{ m}^3 \text{ s}^{-1}$ in 1922, $Q < 13 \text{ m}^3 \text{ s}^{-1}$ in

2014 (see Bulteau et al., 2022 for details), and the main zones of bed degradation were identified.

4. Results

4.1. Fine sediment interstitial storage

4.1.1. Longitudinal pattern

Riverbed storage showed a decreasing trend from upstream to downstream for all size classes considered as fines (silt-clay, and sand, Fig. 4) albeit with high variability in the by-passed reach. Overall, the average silt-clay, and sand, proportions decreased from 0.34 % and 17.8 %, respectively, at UP1, to 0.15 %, and 6.5 % at DS2. Sand is by far the dominant fraction, and exceeded the proportion of silt-clay by one to two orders of magnitude (see Fig. S2 in Supplementary Material). The BPR showed higher proportions of silt, clay and sand than upstream and downstream reaches, demonstrating a local fine sediment enrichment (Fig. 4). D_{16} was rather similar across all sites (20–27 mm), except in the BPR where it fell to 11 mm, confirming the enrichment of the by-pass with finer fractions, as indicated by the surface GSD. This enrichment could be largely explained by the effects of by-passing on hydrology and bed mobility. Sediment tracing provided information on bedload behaviour over all sites, and over a range of discharges involving partial to total mobility of the injected tracers. Table 2 summarises the main results from sediment tracing, which help explaining the spatio-temporal dynamics of the fine sediment. Indeed, computation of the exceedance frequency for moving particles of 2 mm ($Q_{C2\text{mm}}$) showed that sand mobility occurred for only 6.5 % of the time in the BPR, mostly during flood events, while this threshold was surpassed 34 %, 11 %, and 98 % of the time at the UP, DS1, and DS2 sites, respectively.

Through its effects on bed mobility, roughness and near-bed flow conditions, bed armouring seems to influence the FSIS in several ways. The following observations should be considered to be unrelated to the

Table 2

Characteristics of the bedload transport over the study sites. UP = pooled values of UP1 and UP2. BP = pooled values of BP1, BP2 and BP3. $Q_{CD50/84}$: critical discharge to move particles of the sizes D_{50}/D_{84} .

Sites	UP	BP	DS1	DS2	Pi1
n	331	315	334	322	293
Recovery rate (%)	39–47	33–51	12–32	12–36	25–53
$Q_{C2\text{mm}}$ ($\text{m}^3 \text{s}^{-1}$)	15	25	35	10	-
Q_{CD50} ($\text{m}^3 \text{s}^{-1}$)	45–50	55–65	75	80	30
Q_{CD84} ($\text{m}^3 \text{s}^{-1}$)	60–70	70–90	87	120	40
Active Layer Thickness (m)	0.06	0.10	0.19	0.15	0.05

Plan d’Arem dam because they concern reaches both upstream and downstream, as well as the control station on the Pique River. On the one hand, the inter-site variability of FSIS (measured from the “volumetric” cylinder-corer method) was fairly correlated with the bed armouring ratio (measured from “areal” Wolman method). Spearman rank correlation (used because of highly heteroscedastic data) values of the statistical relationship between the armouring ratio and the FSIS were equal to 0.57 for silt and clay, and to 0.55 for sands ($p < 0.01$, Fig. 5A & 5B). These observations corroborate the results from sediment tracing experiments: within the most armoured sections, the bed experiences less frequent full mobility which promotes FSIS. On the other hand, we observed a positive correlation between bed armouring and the standard deviation of silt-clay proportion, confirming the effect of bed structure on the intra-site variability of this fraction ($r(4) = 0.77$, $p = 0.02$; Fig. 5C). This correlation was not significant for the sandy fraction of FSIS ($r(4) = 0.42$, $p = 0.10$).

4.1.2. Temporal dynamics

As a matter of general results description, we observed a remarkable temporal variability in the fine sediment proportion in the bed (Fig. 6A). Each site presented specific FSIS dynamics, according to its position

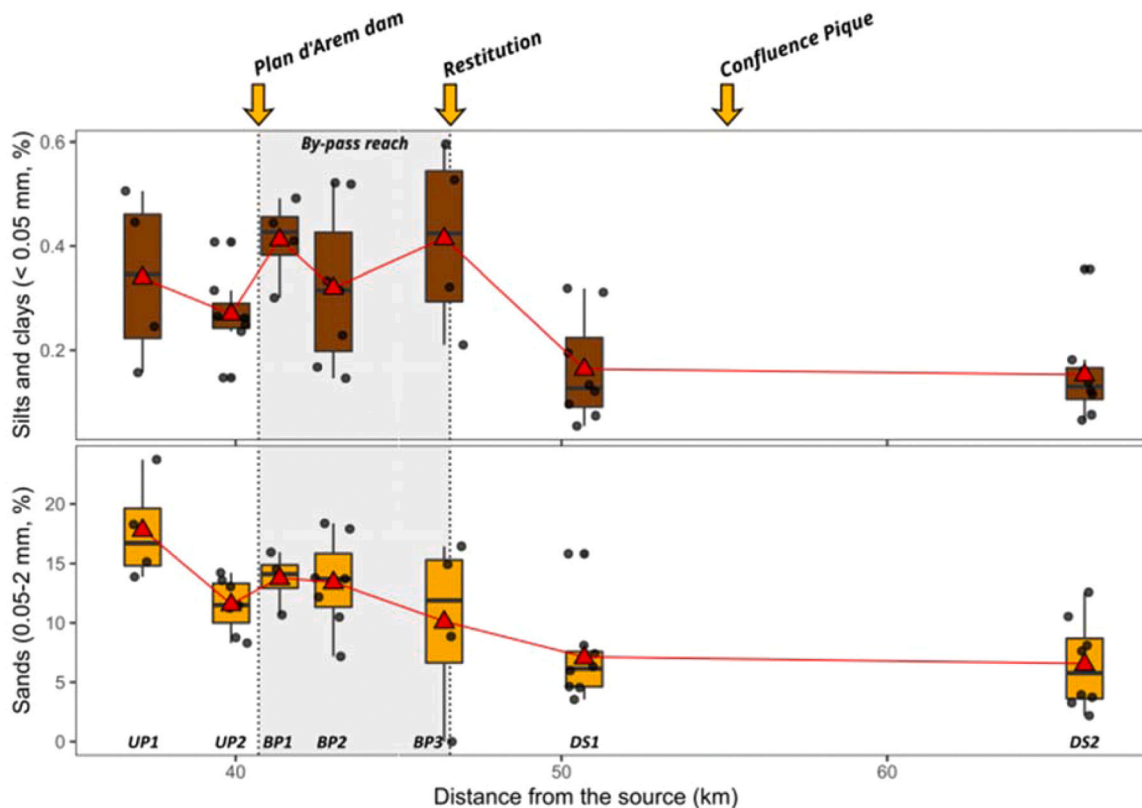


Fig. 4. Longitudinal pattern of fine sediments in the river-bed. Boxplots represent the distribution overall (median, quartiles, 10 and 90 percentiles), black dots represent individual observations, red triangles and red lines represent site-averaged values. UP1 to DS2 represent sites.

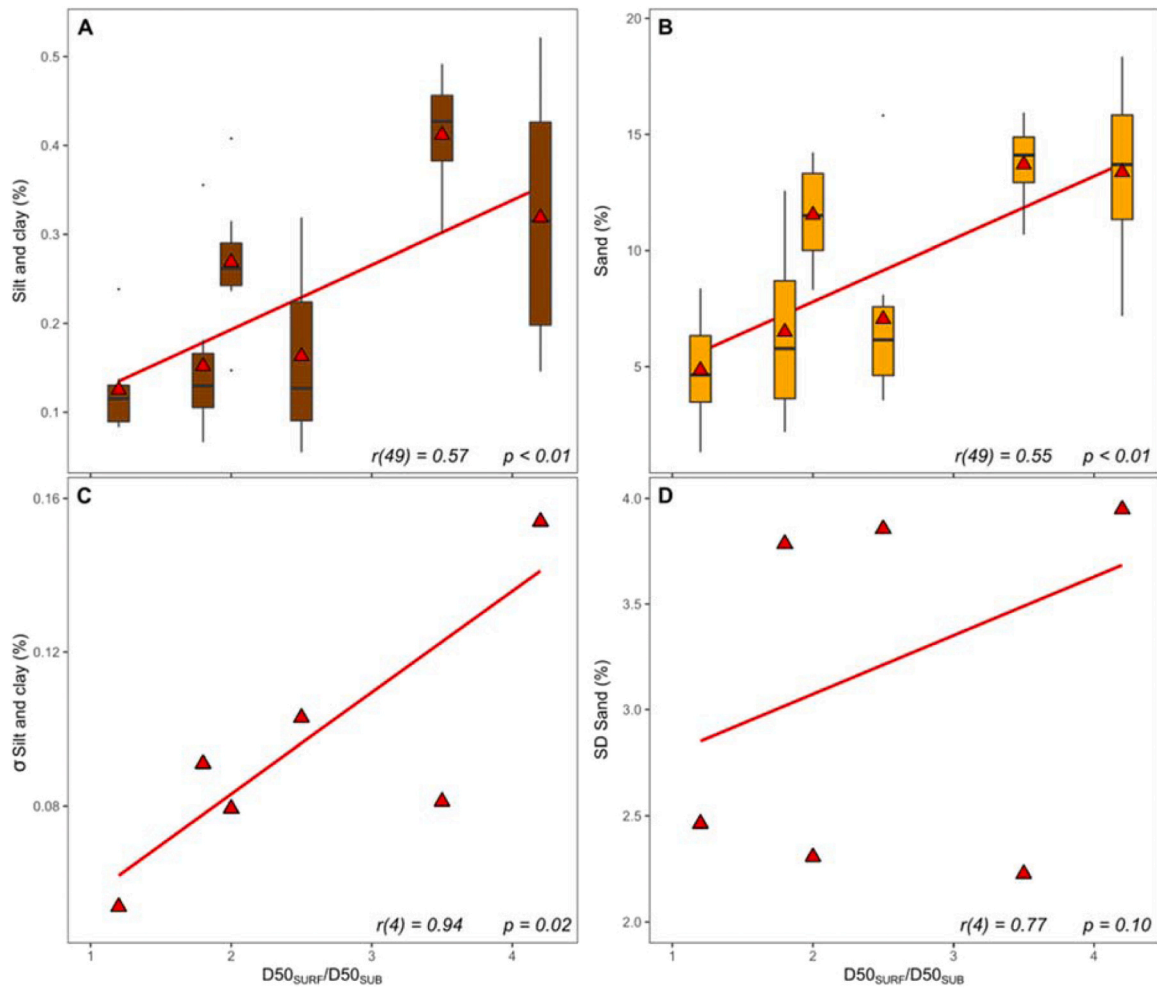


Fig. 5. Effects of bed armoring (i.e. $D50_{\text{surface}}/D50_{\text{subsurface}}$) on inter-site (5A & 5B) and intra-site (5C & 5D) variability of FSIS. σ stands for Standard Deviation. Correlation coefficient $r(df)$ refer to Spearman rank correlation tests, with df = degree of freedom. Red lines simply symbolise a tentative linear relationship.

within the study reach (i.e. upstream of the dam ‘UP’, in the by-passed reach ‘BP’, downstream from the restitution ‘DS’). Within each section, the response of fine sediments to the occurrence of flood events was specific, and apparently related to local geomorphic features (i.e. bed structure controls on bed mobility, see Section 4.1.1. and Bulteau et al., in review). Finally, sand and silt-clay proportions displayed very distinct trends, which may mean that the processes of storage and release were different and occurred independently.

A more extensive investigation of the temporal dynamics of interstitial sands highlights that, independently from the section considered (i.e. local geomorphic features), two main factors seem to influence the response of this fraction to flood events. The first factor is the occurrence of a competent flood event. For all section, competent floods ($Q > Q_{cD84}$) corresponding to flood discharge sufficiently high to trigger drawdown flushing actions at the Plan d’Arem dam resulted in rather low values of sand storage after both the first drawdown episode (23/10/2019; with nondimensional proportion of sand at sampling 5 [P_{S5}^*] equal to 0.10, 0.51 and 0.04 at sections UP, BP and DS, respectively), and the second drawdown episode (13/12/2019 and 20/12/2019; P_{S6}^* equal to 0.10, 0.51 and 0.04 at sections UP, BP and DS, respectively), whereas values were higher at the previous campaign ($P_{S4}^* = 0.50, 0.30$ and 1 at sections UP, BP and DS, respectively; Fig. 6A). Contrarily to the effects of competent flood events, the response of FSIS to smaller floods, typically just sufficient to initiate motion of the surface D_{50} , was site-dependant and less clear. At sections UP and BP, the proportion of sand, although displaying high values before the spring 2019 snow-melt

($P_{S1}^* > 0.75$) increased again with the small floods of May 2019 and reached among the highest values recorded over the study period (i.e. $P_{S2}^* \sim 1$). Interestingly, at the same sections, the response of interstitial sands to spring 2020 snow-melt was different, despite hydrological characteristics of both periods being similar. Proportions of sands, which was rather low at the beginning of the period ($P_{S6}^* < 0.51$), increased at the section UP, and decreased at the section BP (Fig. 6A). Thus, both sections show very similar response to large floods but respond unevenly to smaller events. A second factor arising from these observations and potentially controlling the during-flood decrease of interstitial sand storage is the proportion of sand readily available in the bed before a competent event occurs. Low proportions of interstitial sand before a flood ($P_{PRE}^* < 0.25$; Fig. 6B) lead to either a stable level or an enrichment of sand proportion after the flood ($P_{POST}^* - P_{PRE}^* > 0$; Fig. 6B). Conversely, a relatively high proportion of sand before a flood ($P_{PRE}^* > 0.50$) increases the variability of FSIS response to that event. This variability is controlled by bedload transport characteristics, i.e. partial transport is associated with a high variability in the response of interstitial sands (e.g. UP and BP), whereas full transport leads to systematic decrease in sand proportion (e.g. DS; Fig. 6B).

The behaviour of silt and clay differed from that of sand and also between sites. The proportion of silt and clay is positively correlated with that of sand at sites UP1 and BP1 ($r^2 = 0.6$ and 0.77 , respectively), negatively correlated at BP2 ($r^2 = 0.45$), and did not correlate significantly at the other sites ($r^2 < 0.15$). Downstream from the Plan d’Arem dam, the highest proportions of silt and clay were observed in November

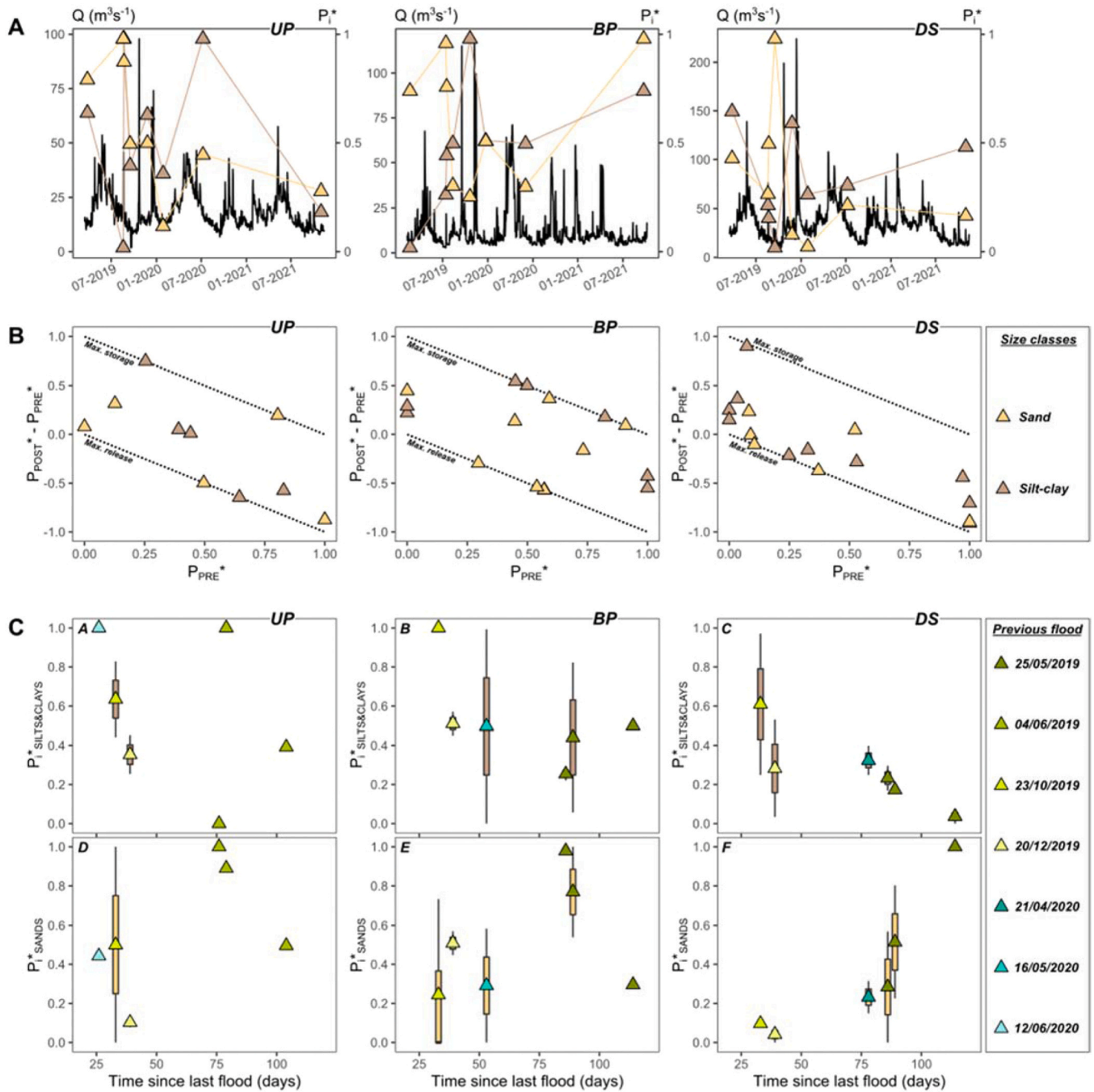


Fig. 6. Temporal dynamics of Fine Sediment Interstitial Storage (FSIS). A. Temporal patterns of FSIS (brown triangles represent silt and clay fraction, yellow triangles represent sand fraction) shown as nondimensional relative changes. B. During-flood changes in silt-clay (brown triangle) and sand (yellow triangle) plotted against the pre-flood FSIS level of each fraction. C. Temporal patterns of post-flood changes in FSIS.

2019, between two competent floods that involved flushing actions, but these proportions dropped after the second competent event (January 2020). This indicates that, if flushing actions may have temporarily increased storage, fines were quickly remobilised. No clear trend was observed in changes in silt and clay over non-competent flood periods. It is worth keeping in mind that surveys S7 (July 2020) and S8 (November 2021) were one and a half years apart, which is a long period considering the high temporal variability of the processes analysed, and which must force us to exercise caution when interpreting the results from that period.

Interesting trends arise from the analysis of post-flood changes in FSIS (Fig. 6C). For this analysis, the values from the first and the last

campaigns (S1 in April 2019 and S8 in November 2021, respectively) were removed (because S1 had no previous flood and S8 no subsequent flood on records). In general, silt-clay and sand proportions displayed opposite post-flood trends. Highest values of silt-clay storage were observed at all sections shortly after a flood occurred, independently from the flood considered (i.e. 26 days after the flood of 12/06/2020 at section UP, 33 days after the flood of 23/10/2019 at sections BP and DS). These values dropped afterwards, to reach a low FSIS level some 76 days after the flood of 04/06/2019 at section UP, 86 days and 114 days after the flood of 25/05/2019 at sections BP and DS, respectively. These results highlight that (1) high levels of silt-clay storage post-flood did not persist and may then be rather associated with a transitory state, with

potentially low risk of bed clogging, and that (2) these fine sediments are more rapidly flushed in the uppermost sections that are coarse and armoured than from lowermost sections which experience frequent full-mobility of the active layer during floods (i.e. with more heterogeneous material and lower bed porosity).

Contrarily to silt-clay, sand storage is at the lowest immediately after a competent event (Fig. 6C), and progressively increases to reach maximum values some 76 days after the flood of 04/06/2019 at section UP, 86 days and 114 days after the flood of 25/05/2019 at sections BP and DS, respectively. We may interpret this increasing trend as an effect of residual sand transport. During a given competent flood, the interstitial sand is exported and leave available pore space. After the flood, residual and intermittent sand transport during small floods and hydropeaks progressively fill available space. This result is consistent with the study of Blaschke et al. (2003), which reports that a new quasi-stable state is reached a few weeks after a flood reset the clogging cycle.

4.2. Longitudinal pattern of water temperature

The longitudinal profile of water temperature was segmented into eight sub-reaches (A-H) characterised by similar gradients and considered as homogeneous (Fig. 7). Upstream from the Plan d’Arem dam, reach A is marked by a negative temperature gradient ($-1^{\circ}\text{C km}^{-1}$), although this may not reflect any significant trend considering the shortness of this reach (~ 700 m). Reach B, corresponding to the reservoir, shows a positive gradient ($+0.32^{\circ}\text{C km}^{-1}$) probably related to high insolation and longer residence time. Water temperature drops at the dam outlet, reducing by approximately 1.4°C . Over reaches C and D, the BPR recorded an important increase in water surface temperature, rising from 13.1°C at the dam outlet to 15°C at the restitution, with the gradient becoming less important heading downstream (Fig. 7A). Note that this observation was not related to water diversion because the dam did not operate on the day of the TIR mapping and the BPR therefore conveyed the entire discharge from upstream. Reach E was marked by a

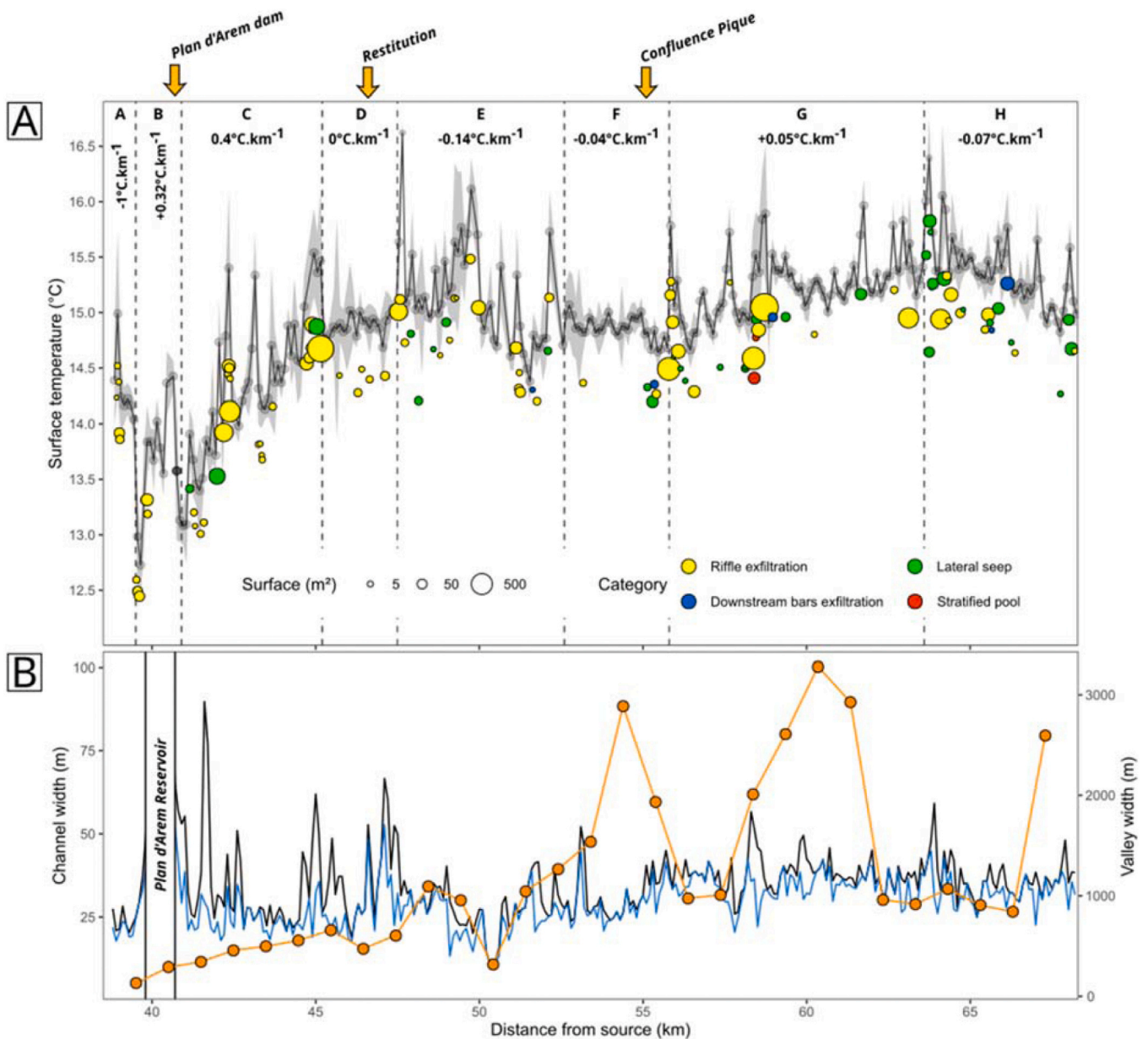


Fig. 7. A. Longitudinal temperature profile and associated cool-water features detected along the study reach (size of dots refer to size of patches, y-positions reflect median temperature of cool-water patches). B. Longitudinal patterns of active (black line) channel width, wetted channel width (blue line), and valley bottom width (orange line and dots).

large variability in water temperature ($\Delta T_{\text{MIN-T}_{\text{MAX}}} = 2.24^{\circ}\text{C}$) and an overall negative gradient of $-0.14^{\circ}\text{C km}^{-1}$, with the highest temperature recorded between RK49 and RK50 due to an old water diversion. From RK52.6 to the downstream limit of the study reach, we identified three reaches characterised by a low temperature gradient ($-0.07^{\circ}\text{C to }+0.05^{\circ}\text{C km}^{-1}$), with locally important variability of about $\pm 1^{\circ}\text{C}$.

Observation of the cool patch types and density provides comprehensive information on riverbed thermal functioning. River morphology exerted substantial effects on the distribution of cool-water patches (see Fig. S1 in Supplementary Material). The highest density of cool-water patches associated with riffle upwelling was observed in the BPR, especially in reach C with $276 \text{ m}^2 \text{ ha}^{-1}$, indicating a zone of rather active exchanges between surface water and the hyporheic zone. We also observed a lower number of cool-water patches over reaches F, G, and H (83, 114, and $116 \text{ m}^2 \text{ ha}^{-1}$, respectively), with an important proportion of patches being attributed to lateral seeps over reach H (44 %, $51 \text{ m}^2 \text{ ha}^{-1}$). The two reaches located at RK53–55 and RK59–62 were characterised by the absence of such patches, which coincided with valley widening (Fig. 7B).

The TIR survey was carried out the 15/09/2019, one day before the campaign S4. At this campaign, FSIS values were moderate at sections UP and BP, comprised between 0.25 and 0.5 for both sand and silt-clay fraction (Fig. 6A). At the same campaign were recorded the highest value of sand storage and the lowest value of silt-clay storage at section DS. Overall, we may state that the day the TIR images were captured, FSIS level was rather representative of a time-integrated average value of storage over the study period, although more belonging to the lower range of observations.

5. Discussion

5.1. Is there interstitial storage of fine sediment downstream from the Plan d'Arem dam?

The FSIS within the coarse sediment matrix of the channel showed a general decreasing downstream trend over the study reach. Fine sediments mostly consisted of sandy material, typically representing 4–20 % of the sample mass, and perhaps even less of the total bed material considering the sampler mouth size and sample truncation. Silt and clay accounted for less than 0.5 % of sample mass, and for an average of 4.7 % of the fines, i.e., probably not very different from typical washload (e.g., Gayraud and Philippe, 2003). These proportions are generally low but in the range of values given in the literature; for example, Gayraud and Philippe (2003) found an average of 1.03 % of silt and clay in the bed material of 15 French streams, Ryan and Packman (2006) showed that silt and clay represented 6–25 % of fines on two streams from an urbanised watershed in the USA, and Descloux, (2011) found that fines represent between 8.3 % (unclogged) and 55.2 % (very clogged) of freeze core samples.

The main effect of the Plan d'Arem dam on FSIS is caused by changes in the local hydraulics through water diversion. This lowers the exceedance frequency for mobility of the finer fractions (e.g. sand), resulting in fine sediment enrichment in the BPR (Impact 1). FSIS drops downstream from the restitution thanks to a restored transport capacity, and remains rather low over the rest of the study reach (Impact 2). Drawdown flushing actions and associated fine sediment releases from the dam may temporarily increase storage, but subsequent floods are sufficiently competent to mobilise bed material and flush the deposited material. As such, FSIS levels are lower after flushing actions than at the end of long low-flow periods. Nevertheless, the role of suspended sediments in controlling riverbed clogging is frequently discussed, and other factors such as connectivity with sediment sources within the basin (Marteau et al., 2018), hydrology (Piqué et al., 2014), and local hydraulics and sediment characteristics (Misset et al., 2019) often exert stronger effects.

The surface GSD was partly independent of the Plan d'Arem dam,

and appeared to be a dominant factor controlling fine sediment storage and release through two main processes. Large structural elements have hiding effects that allow fines to settle and rest under flow conditions that would otherwise lead to their transport in the absence of cobbles and boulders. Moreover, such coarsening also testifies of some local bed armouring, resulting in less frequent and more partial bed mobility during floods. As a consequence, sites with bed armouring show higher FSIS. Additionally, coarse features create local fixed-bed conditions, allowing patches of mobile material to settle within the upper layer. Here, the method used only allowed us to assess how this sieving process affects sediment enrichment within the top layer of the riverbed (i.e., 10 cm). However, we argue that sieving into deeper layers is unlikely in the Garonne River since it would affect hyporheic exchanges (see discussion below), but also because Bulteau et al. (in review) showed that sites with fixed-bed conditions only had a shallow scour layer. Conversely, sites with a smaller surface GSD and better particle sorting show a higher mobility (even total mobility) of bedload and higher scouring ($>15 \text{ cm}$, Table 2). These observations of bedload mobility relate to the specific dynamics of the FSIS behaviour, which shows higher intra-site variability in sites characterised by the presence of large cobbles and boulders, especially for silt and clay. A number of authors reported the importance of bed grain size and distribution (i.e., hiding effect), as well as bed mobility, in the control of incipient deposition and of the depth of fine sediment infiltration (e.g. Wharton et al., 2017), which supports our observations. Coarse beds were shown to promote initial particle deposition and intrusion within the top layer (Evans and Wilcox, 2014). If the poor sorting often observed in transport-limited coarse-bed natural streams leads to reduced porosity (Wooster et al., 2008), it is not the case on the Upper Garonne which experiences a long-standing and structural sediment deficit (Bulteau et al., 2022). Similarly, Gayraud and Philippe (2003) found a significant positive correlation between the sediment sorting index and the proportion of silt-clay ($\rho = 0.30$) and sand ($\rho = 0.77$, where ρ is the Pearson correlation coefficient).

Following our first hypothesis, we can then compare observations from our different sites to separate out the potential effects of the dam on FSIS from other factors. Downstream from Plan d'Arem, FSIS is more affected by the reduction in peak flows than by sediment starvation. As such, the dam and associated drawdown flushing actions do affect FSIS. However, increase in FSIS remains relatively low, (e.g., lower than that observed upstream from the dam at some of the sites with similar bed texture and hydrological conditions) and the grain size characteristics of the fine sediments prevents interstitial storage from impeding hyporheic exchanges.

5.2. Can FSIS be defined as clogging when thermal patterns are examined?

We analysed the longitudinal structure of thermal gradients and the distribution of cool-water patches. Information on the geomorphological setting described by Bulteau et al. (2022) provides elements of interpretation of river temperature patterns. At the large-scale, the shape of the valley (i.e. alternance of tarns and locks, of wide and narrow valley bottom) may cause the river to feed the aquifer where the valley is large, and the groundwater to re-surface where the valley narrows (e.g. Dugdale et al., 2015). The dominant downward direction of exchanges in areas where the valley widens results in a lower density of cool-water patches, but with no impact on thermal gradients apart from a decrease in the local variability of surface temperature (e.g. reach F and middle of reach G, Fig. 7A). At a more local-scale, we identified the Plan d'Arem dam as a key factor controlling downstream surface temperature. The dam outflow is cold, but then rapidly warms up within approximately 4 km, to reach an equilibrium temperature of ca. 14.5°C – 15°C until the downstream end of the study reach. Surface temperature rises locally in areas of heavy ongoing in-channel roadwork (e.g., St Béat village, RK48–50) and upstream of weirs and bridges

(RK56, RK58, and RK64). The by-passed reach which is also located in a wide valley characterised by a fairly wide active channel with a series of riffles displays numerous evidences of upwelling. This reach with significant hyporheic (i.e., vertical) exchanges contrasts with areas of incision further downstream that show more lateral seeps due to outflow of the local aquifer from the banks (i.e., lateral exchanges). While both types of features result in a net inflow into the river, the processes (and potential use/benefits to the biota) are different.

In the light of these different elements, we can state that fine sediment infilling of the riverbed matrix does not impede exchanges between hyporheic water and surface water in the upper Garonne River. Indeed, reaches with high FSIS (e.g., BPR) still host a number of cool-water patches, indicating that storage does not inhibit water exchanges with the hyporheic zone. We make the assumption that because the fine material stored in the riverbed is mostly sandy-granular, it is less likely to alter hydraulic conductivity (Wharton et al., 2017). Similarly, the sediments stored in Plan d'Arem dam present non-cohesive characteristics albeit rather fine-grained (global D_{50} between 1.6 and 5.6 mm, and the fines D_{50} between 0.6 and 0.8 mm, UWITECH, 2014). It is this sediment that is being released during drawdown flushing actions, but its characteristics combined with the relatively high mobility of the riverbed provides the physical support to maintain functional hyporheic exchanges. The bed armouring that is occasionally observed in the study reach is not generalised, explaining the temporal variability of FSIS. A highly armoured and degraded bed would have led to a relatively continuous build-up in fine sediment storage with little or no release of fines (Brunke, 1999) with potentially deleterious effects on hyporheic exchanges.

These observations support our interpretation that fine sediment infilling in the upper Garonne, which can be triggered by drawdown flushing actions, does not generate clogging in the sense that it would impede flow exchanges with the hyporheic zone. In this case, airborne acquisition of temperature data helped interpret whether FSIS should be considered as clogging. These results also underline the need to be very careful when defining clogging solely based on FSIS measurements.

5.3. Lessons learned from a methodological perspective

While the benefits of using multiparameter approaches to assess riverbed clogging is not new (Negreiros et al., 2023), there are still needs to explore new methods to refine our understanding of the processes and its consequences (Seitz, 2020). Here, the coupling of in-field sediment sampling and TIR mapping offered an interesting perspective on such assessment. Field sediment sampling provides a direct and discrete information on riverbed composition and is easily repeatable over time to assess temporal dynamics, whereas the TIR mapping can be used as a proxy to assess whether FSIS can actually be considered as clogging from a more functional (i.e., hyporheic exchanges) perspective. We can use results from the by-passed reach as an illustration of the benefits of our method: based on fine sediment sampling only, this site could have been considered as suffering from high level of clogging because it showed high FSIS values, yet the observations of functional water exchanges proved otherwise.

FSIS is a complex problem to assess because it is time and space contingent. To control these conditions, a strategy based on inter-site comparison is needed with consideration of a range of (1) spatial conditions in terms of grain size, relative position to the dam, and water diversion, and of (2) a range of temporal conditions in terms of sediment mobility, hydrology, and dam operation. Acknowledging and integrating the different forms of variability in the sampling strategy is the only way to properly assess the respective effects of all these factors and determine their relative contribution in controlling FSIS.

The variety of morphological contexts and human disturbances found in rivers does not always allow for such distinction on the basis of spatial segmentation and inter-comparison of homogeneous reaches, and therefore other complementary approaches are needed to provide

additional information to that provided by the spatio-temporal framework. In our case, although the observed effects of surface GSD on FSIS were apparently independent from the dam, *in-situ* study of the bedload behaviour and calculation of critical discharges for various size classes were required to distinguish the effects of surface GSD from those of water diversion, especially given that the sections with the coarsest surface layer on both the Garonne (Control 1, Impact 1) and Pique (Control 3) rivers were also the by-passed sections. The repetition of high-frequency FSIS measurements can help to overcome high intra-site variability and to improve the robustness of the method. Finally, a more detailed assessment of the direct unitary effects of drawdown flushing actions and their persistence through time and space, which could not be conducted here given the limited number of field campaigns, would provide further information on how dam operation and management could further help control the dynamics of fine sediment storage.

6. Conclusion

The present study aimed to characterise the Fine Sediment Interstitial Storage (i.e. FSIS, encompassing sand, silt and clay) and release processes in the vicinity of a RoR dam, and their potential role in inducing riverbed clogging. This was accomplished by coupling sediment sampling with the acquisition of high resolution airborne TIR imagery. This innovative approach, in line with previous recommendations to use multi-parameter approaches when studying riverbed clogging, relied on a spatio-temporal sampling framework to identify and assess the relative contribution of individual factors on the control of interstitial fine sediment dynamics. Our two working hypotheses, i.e., that (1) the effects of the dam on riverbed infilling could be explained by geomorphological and hydrological parameters, and that (2) TIR imagery could help interpreting whether FSIS effectively generates clogging, were validated. The upper reach of the Garonne River is subjected to contrasting levels of FSIS, varying both spatially and temporally, and sometimes reaching relatively high levels. However, none of the sites were determined as suffering from 'clogged' conditions according to the definition given in the introduction (analysed here 'through the lens' of hyporheic exchanges). Drawdown flushing plays a role in maintaining sediment dynamics downstream from dams by providing flood-like discharges. In addition, flushing contributes to limiting sediment infilling in the reservoir while providing material downstream in an otherwise sediment-starved channel. Although encouraging results such as the ones presented here offer interesting management perspectives, the authors would like to emphasise the unique character of each study site, and the requirement for careful in-situ analysis and diagnosis before implementing any new dam management procedure.

CRedit authorship contribution statement

Hervé Piégay: Writing – review & editing, Supervision, Project administration, Methodology, Funding acquisition, Conceptualization. **Philippe Valette:** Writing – review & editing, Supervision. **Emmanuel Chapron:** Writing – review & editing, Supervision. **Ramon J. Batalla:** Writing – review & editing, Supervision, Funding acquisition, Conceptualization. **Baptiste Marteau:** Writing – review & editing, Investigation, Formal analysis. **BULTEAU THEO:** Writing – review & editing, Writing – original draft, Methodology, Investigation, Formal analysis, Conceptualization.

Declaration of Competing Interest

The authors declare that they have no known competing financial interests or personal relationships that could have appeared to influence the work reported in this paper.

Data Availability

Data will be made available on request.

Acknowledgements

Agence Nationale de la Recherche (French National Research Agency), Grant/Award Number: EUR H2O'Lyon (ANR-17-EURE0018); Spanish General Directorate for Water (DGA-MITERD), Grant/Award Number: 20223TE012IGME-CSIC; Economy and Knowledge Department of the Catalan Government; Région Auvergne-Rhône-Alpes; Électricité de France; Université de Lyon; Ministry of Science, Innovation and Universities.

Appendix A. Supporting information

Supplementary data associated with this article can be found in the online version at [doi:10.1016/j.ancene.2024.100444](https://doi.org/10.1016/j.ancene.2024.100444).

References

- Annandale, G.W., 2013. Quenching the Thirst: Sustainable Water Supply and Climate Change. CreateSpace, North Charleston, S. C.
- Bartholow, J.M., 1991. A modeling assessment of the thermal regime for an urban sport fishery. *Environ. Manag.* 15, 833–845.
- Blaschke, A.P., Steiner, K.-H., Schmalfluss, R., Gutknecht, D., Sengschmitt, D., 2003. Clogging processes in hyporheic interstices of an impounded river, the Danube at Vienna, Austria. *Intern. Rev. Hydrobiol.* 88 (3-4), 397–413. <https://doi.org/10.1002/iroh.200390034>.
- Bloesch, J., Burns, N.M., 1979. A critical review of sedimentation trap technique. *Zool. Hydrod.* 42, 15–55.
- Boutault, F., 2020. Etude de l'impact cumulé des facteurs d'anthropisation sur la Dordogne moyenne et préconisations en vue de la restauration écologique du cours d'eau. University of Lyon, France. Ph.D. Dissertation. DOI: [10.13140/RG.2.2.10836.32643](https://doi.org/10.13140/RG.2.2.10836.32643).
- Bretschko, G., Klemens, W., 1986. Quantitative methods and aspects in the study of the interstitial fauna of running waters. *Stygologia* 2, 279–316.
- Brousse, G., Liébault, F., Arnaud-Fassetta, G., Vázquez-Tarrío, D., 2018. Experimental bed active-layer survey with active RFID scour chains: Example of two braided rivers (the Drac and the Vénéon) in the French Alps. *E3S Web Conf.* 40, 04016. <https://doi.org/10.1051/e3sconf/20184004016>.
- Brunke, M., 1999. Colmation and depth filtration within streambeds: retention of particles in hyporheic interstices. *Int. Rev. Hydrobiol.* 84, 99–117.
- Brunke, M., Gonser, T., 1997. The ecological significance of exchange processes between rivers and groundwater. *Freshw. Biol.* 37, 1–33.
- Buffington, J.M., 1996. An alternative method for determining subsurface grain size distributions of gravel-bedded river. *Am. Geophys. Union 1996 Fall Meet., Suppl. Eos. AGU Trans.* 77 (46).
- Bulteau, T., Batalla, R.J., Chapron, E., Valette, P., Piégay, H., 2022. Geomorphic effects of a run-of-the-river dam in a multi-driver context: the case of the Upper Garonne (Central Pyrenees). *Geomorphology* 408, 108243. <https://doi.org/10.1016/j.geomorph.2022.108243>.
- Bulteau, T., Vázquez-Tarrío, D., Batalla, R.J., Piégay, H., in review. A multi-site and hypothesis-driven approach to identify controls on the bedload transport regime of an anthropised gravel-bed river. *Earth Surface Processes and Landforms*.
- Bunte, K., Abt, S., 2001. Sampling surface and subsurface particle-size distributions in wadable gravel- and cobble-bed streams for analyses in sediment transport, hydraulics and streambed monitoring. In: General Technical Report RMRS-GTR-74. U.S. Department of agriculture, Forest service, Rocky mountain research station, Fort Collins, CO, 428 p.
- Caisse, D., 2006. The thermal regime of rivers: a review. *J. Freshw. Biol.* 51, 1389–1406. <https://doi.org/10.1111/j.1365-2427.2006.01597.x>.
- Collins, A.L., Zhang, Y., 2016. Exceedance of modern 'background' fine-grained sediment delivery to rivers due to current agricultural land use and uptake of water pollution mitigation options across England and Wales. *Environ. Sci. Policy* 61, 61–73. <https://doi.org/10.1016/j.envsci.2016.03.017>.
- Coulombe-Pontbriand, M., Lapointe, M., 2004. Geomorphic controls riffle substrate quality, and spawning site selection in two semi-alluvial salmon rivers in the Gaspé Peninsula, Canada. *River Res Appl.* 20, 577–590. <https://doi.org/10.1002/rra.768>.
- Descloux, S., 2011. Le colmatage minéral du lit des cours d'eau: méthode d'estimation et effets sur la composition et la structure des communautés d'invertébrés benthiques et hyporhéiques. University of Lyon, France. Ph. D. Dissertation.
- Dugdale, S.J., 2016. A practitioner's guide to thermal infrared remote sensing of rivers and streams: recent advances, precautions and considerations. *Wiley Interdiscip. Rev.: Water* 3 (2), 251–268. <https://doi.org/10.1002/wat2.1135>.
- Dugdale, S.J., Bergeron, N.E., St-Hilaire, A., 2015. Spatial distribution of thermal refuges analysed in relation to riverscape hydromorphology using airborne thermal infrared imagery. *Rem. Sens Environ.* 160, 43–55. <https://doi.org/10.1016/j.rse.2014.12.021>.
- Evans, E., Wilcox, C., 2014. Fine sediment infiltration dynamics in a gravel-bed river following a sediment pulse. *River Res. Appl.* 30, 372–384. <https://doi.org/10.1002/rra.2647>.
- Gayraud, S., Herouin, E., Philippe, M., 2002. Colmatage minéral du lit des cours d'eau: revue bibliographique des mécanismes et des conséquences sur les habitats et les peuplements de macroinvertébrés. *Bull. Fr. Pêche Piscic.* 365/366, 339–355.
- Gayraud, S., Philippe, M., 2003. Influence of bed-sediment features on the interstitial habitat available for macroinvertebrates in 15 French streams. *Int. Rev. Hydrobiol.* 88 (1), 77–93. <https://doi.org/10.1002/iroh.200390007>.
- Greig, S.M., Sear, D.A., Carling, P.A., 2005. The impact of fine sediment accumulation on the survival of incubating salmon progeny: Implications for sediment management. *Sci. Total Environ.* 344, 241–258.
- Hockey, J.B., Owens, I.F., Tapper, N.J., 1982. Empirical and theoretical models to isolate the effect of discharge on summer water temperatures in the Hurunui River. *J. Hydrol. (N. Z.)* 21, 1–12.
- Killick, R., Beaulieu, C., Taylor, S., Hullait, H., 2021. EnvCpt: Detection of Structural Changes in Climate and Environment Time Series year. R package version 1.1.3.
- Kondolf, G.M., Gao, Y., Annandale, G.W., Morris, G.L., Jiang, E., Zhang, J., Cao, Y., Carling, P., Fu, K., Guo, Q., Hotchkiss, R., Peteuil, C., Sumi, T., Wang, H.-W., Wang, Z., Wei, Z., Wu, B., Wu, C., Yang, C.T., 2014. Sustainable sediment management in reservoirs and regulated rivers: Experiences from five continents. *Earth's Future* 2, 256–280. <https://doi.org/10.1002/2013EF00184>.
- Lambert, C.P., Walling, D.E., 1988. Measurement of channel storage of suspended sediment in a gravel-bed river. *Catena* 15, 65–80. [https://doi.org/10.1016/0341-8162\(88\)90017-3](https://doi.org/10.1016/0341-8162(88)90017-3).
- Liébault, F., Lallias-Tacon, S., Cassel, M., Talaska, N., 2013. Long profile responses of alpine braided rivers in SE France. *River Res. Appl.* 29, 1253–1266.
- Loire, R., Piégay, H., Malavoi, J.-R., Beche, L.A., Dumoutier, Q., Mosseri, J., Kerjean, C., 2019. Unclogging improvement based on interdate and interreach comparison of water release monitoring (Durance, France). *River Res Appl.* 35 (8), 1107–1118. <https://doi.org/10.1002/rra.3489>.
- Loire, R., Piégay, H., Malavoi, J.-R., Kondolf, G.M., Bèche, L.A., 2021. From flushing flows to (eco)morphogenic releases: evolving terminology, practice, and integration into river management. *Earth-Sci. Rev.* 213, 103475. <https://doi.org/10.1016/j.earscirev.2020.103475>.
- López-Tarazón, J.A., Batalla, R.J., Vericat, D., 2011. In-channel sediment storage in a highly erodible catchment: the River Isábena (Ebro Basin, Southern Pyrenees). *Z. Geomorphol.* 55 (3), 365–382. <https://doi.org/10.1127/0372-8854/2011/0045>.
- Marteau, B., Batalla, R.J., Vericat, D., Gibbins, C., 2018. Asynchronicity of fine sediment supply and its effects on transport and storage in a regulated river. *J. Soils Sediment.* 18 (7), 2614–2633. <https://doi.org/10.1007/s11368-017-1911-1>.
- Marteau, B., Chandresris, A., Michel, K., Vaudor, L., Piégay, H., 2022b. Riparian shading mitigates water warming but cannot revert thermal alteration in lowland rivers. *Earth Surf. Process. Landf.* 47 (9), 2209–2229. <https://doi.org/10.1002/esp.5372>.
- Marteau, B., Michel, K., Piégay, H., 2022a. Can gravel augmentation restore thermal functions in gravel-bed rivers? A need to assess success within a trajectory-based before-after control-impact framework. *Hydrol. Process.* 36 (2), e14480. <https://doi.org/10.1002/hyp.14480>.
- McNeil, W.J., Ahnell, W.H., 1964. Success of Pink Salmon spawning relative to size of spawning bed material. United States Fish and Wildlife Service, Special Scientific Report-Fisheries No. 469.
- Misset, C., Recking, A., Legout, C., Viana-Bandeira, B., Poiré, A., 2021. Assessment of fine sediment river bed stocks in seven Alpine catchments. *Catena* 196, 104916. <https://doi.org/10.1016/j.catena.2020.104916>.
- Misset, C., Recking, A., Navratil, O., Legout, C., Poiré, A., Cazilhac, M., Briguet, V., Esteves, M., 2019. Quantifying bed-related suspended load in gravel bed rivers through an analysis of the bedload-suspended load relationship. *Earth Surf. Process. Landf.* 44 (9), 1722–1733. <https://doi.org/10.1002/esp.4606>.
- Morris, G.L., Annandale, G., Hotchkiss, R., 2008. Reservoir Sedimentation. In: *Sedimentation Engineering: Processes, Measurements, Modeling, and Practice*. Am Soc of Civil Engineers, Reston, VA, USA, pp. 579–612.
- Negreiros, B., Aybar Galdos, A., Seitz, L., Noack, M., Schwindt, S., Wiprecht, S., Haun, S., 2023. A multi-parameter approach to quantify riverbed clogging and vertical hyporheic connectivity. *River Res Appl.* 39, 1659–1666. <https://doi.org/10.1002/rra.4145>.
- Noack, M., 2021. Clogging of riverbeds – from complex field conditions to isolated processes in the laboratory. *Publ. Inst., Pol. Acad. Sci.* 434 (E-11), 21–23. https://doi.org/10.25171/InstGeoph_PAS_Pubs-2021-009.
- Owens, P.N., Batalla, R.J., Collins, A.J., Gomez, B., Hicks, D.M., Horowitz, A.J., Kondolf, G.M., Marden, M., Page, M.J., Peacock, D.H., Petticrew, E.L., Salomons, W., Trustrum, N.A., 2005. Fine-grained sediment in river systems: environmental significance and management issues. *River Res Appl.* 21 (7), 693–717. <https://doi.org/10.1002/rra.878>.
- Packman, A.I., MacKay, J.S., 2003. Interplay of stream-subsurface exchange, clay particle deposition, and streambed evolution. *Water Res. Res.* 39 (4), 1097. <https://doi.org/10.1029/2002WR001432>.
- Piqué, G., López-Tarazón, J.A., Batalla, R.J., 2014. Variability of in-channel sediment storage in a river draining highly erodible areas (the Isábena, Ebro Basin). *J. Soils Sediment.* 14, 2031–2044. <https://doi.org/10.1007/s11368-014-0957-6>.
- Poole, G.C., 2010. Stream hydrogeomorphology as a physical science basis for advances in stream ecology. *J. North Am. Benthol. Soc.* 29 (1), 12–25. <https://doi.org/10.1899/08-070.1>.
- Raus, D., Moulin, F., Eiff, O., 2019. The impact of coarse-grain protrusion on near-bed hydrodynamics. *J. Geophys. Res.: Earth Surf., Am. Geophys. Union* 124 (7), 1854–1877. <https://doi.org/10.1029/2018JF004751>.

- Recking, A., 2016. A generalized threshold model for computing bed load grain-size distribution. *Water Resour. Res.* 52 (12), 9274–9289. <https://doi.org/10.1002/2016WR018735>.
- Rex, J.F., Petticrew, E.L., 2011. *Fine Sediment Deposition at Forest Road Crossings: An Overview and Effective Monitoring Protocol*. Manning, A., 2011. *Sediment transport in aquatic environments*. IntechOpen, p. 348. ISBN 9789535149224.
- Rice, S., Church, M., 1998. Grain-size along two gravel bed river: statistical variations, spatial patterns and sedimentary links. *Earth Surf. Process. Landf.* 23, 345–363. [https://doi.org/10.1002/\(SICI\)1096-9837\(199804\)23:4<345::AID-ESP850>3.0.CO;2-B](https://doi.org/10.1002/(SICI)1096-9837(199804)23:4<345::AID-ESP850>3.0.CO;2-B).
- Roux, C., Alber, A., Bertrand, M., Vaudor, L., Piégay, H., 2015. "Fluvial Corridor": a new ArcGis Toolbox Package for multiscale riverscape exploration. *Geomorphology* 242, 29–37. <https://doi.org/10.1016/j.geomorph.2014.04.018>.
- Ryan, R.J., Packman, A.I., 2006. Changes in streambed sediment characteristics and solute transport in the headwaters of Valley Creek, an urbanized watershed. *J. Hydrol.* 323, 74–91. <https://doi.org/10.1016/j.jhydrol.2005.06.042>.
- Schälchli, U., 1992. The clogging of coarse gravel river beds by fine sediment. *Hydrobiologia* 235/236, 189–197.
- Seitz, L., 2020. Development of new methods to apply a multi-parameter approach – A first step towards the determination of colmatation. University of Stuttgart. Germany. Ph. D. Dissertation.
- Sinokrot, B.A., Gulliver, J.S., 2000. In-stream flow impact on river water temperatures. *J. Hydraul. Res.* 38, 339–349.
- Soulsby, C., Youngson, A.F., Moir, H.J., Malcolm, I.A., 2001. Fine sediment influence on salmonid spawning habitat in a lowland agricultural stream: a preliminary assessment. *Sci. Tot Env* 265, 295–307.
- Staudt, F., Mullarney, J.C., Pilditch, C.A., Huhn, K., 2017. The rôle of grain-size ratio in the mobility of mixed granular beds. *Geomorphology* 278, 314–328. <https://doi.org/10.1016/j.geomorph.2016.11.015>.
- Torgersen, C.E., Ebersole, J.L., Keenan, D.M., 2012. *Primer for identifying cold-water refuges to protect and restore thermal diversity in riverine landscapes*. EPA Sci. Guid. Handb. (Febr.) 91. EPA 910-c-12-001.
- Trimble, S.W., 1983. A sediment budget for Coon Creek basin in the Driftless Area, Wisconsin, 1853-1977. *Am. J. Sci.* 283 (5), 454–474. <https://doi.org/10.2475/ajs.283.5.454>.
- UWITECH, 2014. Carottage cryogénique 2014. EDF R&D. Technical report. 4 p.
- Vázquez-Tarrío, D., Fernández-Iglesias, E., Fernández García, Marquínez, J., 2019. Quantifying the variability in flow competence and streambed mobility with water discharge in a gravel-bed channel: river Esla, NW Spain. *Water* 11, 2662. <https://doi.org/10.3390/w11122662>.
- Walling, D.E., Moorehead, P.W., 1989. The particle size characteristics of fluvial suspended sediment: an overview. *Hydrobiologia* 176/177, 125–149.
- Wang, H.W., Kondolf, G.M., 2014. Upstream sediment-control dams: Five decades of experience in the rapidly-eroding Dahan River Basin, Taiwan. *J. Am. Water Resour. Assoc.* <https://doi.org/10.1111/jawr.12141>.
- Wawrzyniak, V., Piégay, H., Allemand, P., Vaudor, L., Goma, R., Grandjean, P., 2016. Effects of geomorphology and groundwater level on the spatio-temporal variability of riverine cold water patches assessed using thermal infrared (TIR) remote sensing. *Remote Sens. Environ.* 175, 337–348. <https://doi.org/10.1016/j.rse.2015.12.050>.
- Wharton, G., Mohajeri, S.H., Righetti, M., 2017. The pernicious problem of streambed colmatation: a multi-disciplinary reflection on the mechanisms, causes, impacts, and management challenges. *WIREs Water* 4 (5), e1231. <https://doi.org/10.1002/wat2.1231>.
- Wolman, M.G., 1954. A method of sampling coarse river bed material. *Trans. Am. Geophys. Union* 35 (6), 951–956. <https://doi.org/10.1029/TR035i006p00951>.
- Wood, P.J., Armitage, P.D., 1997. Biological effects of fine sediment in the lotic environment. *Environ. Manag* 21 (2), 203–217. <https://doi.org/10.1007/s002679900019>.